Earth and Planetary Science Letters 593 (2022) 117681

Contents lists available at ScienceDirect

Earth and Planetary Science Letters

www.elsevier.com/locate/epsl

$\Delta^{13}CH_3D$ and $\Delta^{12}CH_2D_2$ signatures of methane aerobically oxidized by *Methylosinus trichosporium* with implications for deciphering the provenance of methane gases

Sebastian J.E. Krause [a,*], Jiarui Liu [a], Edward D. Young [a], Tina Treude [a,b,**]

[a] Department of Earth, Planetary and Space Sciences, University of California, Los Angeles, Los Angeles CA 90095, USA
[b] Department of Atmospheric and Oceanic Sciences, University of California, Los Angeles, Los Angeles CA 90095, USA

ARTICLE INFO

Article history:
Received 21 December 2021
Received in revised form 6 June 2022
Accepted 10 June 2022
Available online xxxx
Editor: L. Coogan

Keywords:
methane isotopologues
isotopic fractionation
high-resolution mass spectrometry
aerobic methane-oxidizing bacteria

ABSTRACT

Aerobic oxidation of methane (MOx) is an important biologically mediated process that consumes methane in a wide range of environments. Here we report results of culture experiments with the aerobic methane-oxidizing bacterium *Methylosinus trichosporium* (OB3b) that are used to characterize the mass-18 isotopologue ($\Delta^{13}CH_3D$ and $\Delta^{12}CH_2D_2$) signatures of MOx in residual methane gases. MOx activity was confirmed by simultaneous decrease of methane and oxygen in the bulk gas headspace. Bulk carbon ($^{13}C/^{12}C$) and hydrogen (D/H) isotope ratios of the methane gas increased while both $\Delta^{13}CH_3D$ and $\Delta^{12}CH_2D_2$ decreased as the oxidation proceeded. The corresponding fractionation factors (α) calculated from our experimental results are 0.98485 ± 0.00006 for $^{13}C/^{12}C$, 0.7265 ± 0.0010 for D/H, 0.7141 ± 0.0011 for $^{13}CH_3D/^{12}CH_4$, and 0.4757 ± 0.0023 for $^{12}CH_2D_2/^{12}CH_4$. Deviations of the mass-18 fractionation factors from the Rule of the Geometric Mean (RGM) expressed as γ values are 0.9981 ± 0.0017 for $^{13}CH_3D/^{12}CH_4$ and 0.9013 ± 0.0045 for $^{12}CH_2D_2/^{12}CH_4$. Our α and γ values suggest that while MOx fractionates $^{13}CH_3D$ within error of the RGM, the $\Delta^{13}CH_3D$ and $\Delta^{12}CH_2D_2$ trajectories are very sensitive to even small deviations in $^{13}CH_3D/^{12}CH_4$ from the RGM. Fractionation of $^{12}CH_2D_2$ deviates considerably from RGM, and this causes dramatic and robust effects on the trajectories of residual methane in $\Delta^{13}CH_3D$ vs. $\Delta^{12}CH_2D_2$ space. Our models suggest that $\Delta^{13}CH_3D$ and $\Delta^{12}CH_2D_2$ could potentially mimic microbial methanogenesis signatures in an environment that exhibits a strong Rayleigh Distillation process with little to no replenishment of methane during oxidation. However, in closed or open systems where oxidation is attended by simultaneous methane production, we find that modest increases in $\Delta^{13}CH_3D$ and dramatic increases in $\Delta^{12}CH_2D_2$ are to be expected, thus resulting in isotopologue signatures distinct from microbial methanogenesis. The overall trend in these conditions suggest that methane altered by MOx is distinguishable from other methane sources in $\Delta^{13}CH_3D$ and $\Delta^{12}CH_2D_2$ space.

1. Introduction

Understanding the sources and sinks of methane gas has relevance for many research areas. Methane is an important energy source (Demirbas, 2006), a promising extraterrestrial biosignature (Bouquet et al., 2015; Yung et al., 2018), and a potent greenhouse gas with increasing atmospheric concentrations (Saunois et al., 2016).

Methane sources are either microbial, thermogenic, or abiotic. Microbial methane is produced anaerobically from organic matter by archaea (Whiticar, 1999), aerobically from methylphosphonate by cyanobacteria (Karl et al., 2008), and by groups of fungi (Lenhart et al., 2012). Thermogenic methane is derived from thermal cracking of organic matter (Schoell, 1980, and references therein). Abiotic methane is formed through water-rock interactions (Etiope and Schoell, 2014; Etiope and Sherwood Lollar, 2013).

In the atmosphere, methane is oxidized to CO_2 by hydroxyl radicals (90%) (Reeburgh, 2007). Before emission into the atmosphere, methane can be consumed by microbial aerobic (MOx) or anaer-

* Corresponding author.
** Corresponding author at: Department of Earth, Planetary and Space Sciences, University of California, Los Angeles, Los Angeles CA 90095, USA.
E-mail addresses: sjkrause@g.ucla.edu (S.J.E. Krause), ttreude@g.ucla.edu (T. Treude).

https://doi.org/10.1016/j.epsl.2022.117681
0012-821X/

obic oxidation of methane (AOM). MOx, the focus of this study, consumes methane with oxygen according to:

$$CH_4 + 2O_2 \rightarrow CO_2 + 2H_2O. \quad (1)$$

MOx is an important methane sink in a wide range of environments, including soils (Henckel et al., 2000), freshwater lakes (Guggenheim et al., 2020), and oceanic waters overlying cold seeps (Boetius and Wenzhöfer, 2013; Steinle et al., 2015; Valentine et al., 2001). It is mediated by different groups of aerobic methane-oxidizing bacteria, which use methane as their carbon source (Hanson and Hanson, 1996; Murrell, 2010).

Isotope ratios of carbon ($^{13}C/^{12}C$) and hydrogen (D/H) have been used to distinguish methane source pathways (Etiope and Sherwood Lollar, 2013; Schoell, 1988; Whiticar, 1999, 2020), as well as sink mechanisms (Barker and Fritz, 1981; Coleman et al., 1981; Whiticar, 1999, 2020). Microbially-produced methane is strongly depleted in the heavy carbon and hydrogen isotopes (Claypool and Kaplan, 1974; Rayleigh, 1896; Whiticar, 2020). By virtue of the same principles, methane oxidation preferentially consumes the isotopically lighter methane, leaving behind the isotopically heavier methane in the residual pool. This heavy isotope signature of oxidation has been demonstrated in environmental (Barker and Fritz, 1981; Coleman et al., 1981) and pure culture studies with aerobic methane-oxidizing bacteria (Feisthauer et al., 2011; Templeton et al., 2006; Wang et al., 2016). While carbon and hydrogen isotopes have proved useful for unraveling the formation and subsequent processing of methane gases, substantial overlap in the bulk isotope signatures has led to ambiguity surrounding methane sources and sinks (Whiticar, 1999, 2020).

Recent technological advancements enabled application of two mass-18 doubly-substituted isotopologues of methane, $^{13}CH_3D$ (Ono et al., 2014) and $^{12}CH_2D_2$ measured separately (Young et al., 2017, 2016) or together ($^{13}CH_3D$ + $^{12}CH_2D_2$) (Stolper et al., 2014), to help resolve some of these ambiguities arising from the use of bulk isotope ratios alone. The potential utility of these rare isotopologues as tracers of methane formation and destruction is evidenced in a recent study of methane in serpentinites of the Samail Ophiolite in Oman (Nothaft et al., 2021). In the study, bulk isotope ratios ($\delta^{13}C$ and δD) suggest that some methane is abiotic in origin, while mass-18 isotopologue measurements indicate that it is microbial (Nothaft et al., 2021; Young, 2019). However, this conclusion is tempered by the need to understand more thoroughly the effects of oxidation on rare isotopologue abundances.

Multiply-substituted isotopologues have been used as intramolecular geothermometers to determine CH_4 formation temperatures, because their abundances are dependent on temperature. This dependence is well known on the basis of theory (Liu and Liu, 2016; Webb and Miller III, 2014) and has been validated by measurements (Ono et al., 2014; Wang et al., 2020; Young et al., 2017). The temperature dependence is expressed in the form of the exchange reactions between isotopologues, yielding the two doubly-substituted isotopologues by the reactions

$$^{13}CH_4 + {}^{12}CH_3D \leftrightarrow {}^{12}CH_4 + {}^{13}CH_3D \quad (2)$$

and

$$2\,{}^{12}CH_3D \leftrightarrow {}^{12}CH_2D_2 + {}^{12}CH_4. \quad (3)$$

The equilibrium constants for these exchange reactions in the limit of high temperature are (e.g., Young et al., 2017)

$$k_{Eq,^{13}CH_3D} = \frac{4X\left(^{13}C\right)\left(X\left(H\right)\right)^3 X\left(D\right) X\left(^{12}C\right)\left(X\left(H\right)\right)^4}{4X\left(^{12}C\right)\left(X\left(H\right)\right)^3 X\left(D\right) X\left(^{13}C\right)\left(X\left(H\right)\right)^4} = 1 \quad (4)$$

and

$$k_{Eq,^{12}CH_2D_2} = \frac{6X\left(^{12}C\right)\left(X\left(H\right)\right)^2 X\left(D\right)^2 \left(X\left(H\right)\right)^4}{\left[4X\left(^{12}C\right)\left(X\left(H\right)\right)^3 X\left(D\right)\right]^2} = \frac{3}{8}, \quad (5)$$

where $X(i)$ are the atomic fractions of the indicated isotopes i comprising the methane isotopologues (e.g., $X(^{13}C) = {}^{13}C/({}^{12}C+{}^{13}C)$ and $X(D) = D/(H+D)$, etc.) and the factor of 3/8 is a reflection of the different symmetry numbers of the isotopologues in reaction (3). As temperatures decrease, the lower energies of the intramolecular bonds involving the heavier isotopes become more important, resulting in higher relative abundances of the clumped species and departures from this purely statistical distribution of isotopes. The deviations in the relative abundances of the rare, mass-18 isotopologues relative to the high-temperature limit are expressed using the notation

$$\Delta_{^{13}CH_3D} = 10^3\left(\frac{X\left(^{13}CH_3D\right)}{X\left(^{13}CH_3D\right)_{stochastic}} - 1\right) \quad (6)$$

and,

$$\Delta_{^{12}CH_2D_2} = 10^3\left(\frac{X\left(^{12}CH_2D_2\right)}{X\left(^{12}CH_2D_2\right)_{stochastic}} - 1\right), \quad (7)$$

where $X(^{13}CH_3D)$ represents the molecular fraction of $^{13}CH_3D$ in the methane gas, and so forth, and where stochastic abundances are obtained by treating the relative concentrations of the isotopic species as probabilities, as in Equations (4) and (5), yielding

$$X\left(^{13}CH_3D\right)_{stochastic} = 4X\left(^{13}C\right)X(D)X(H)^3 \quad (8)$$

and

$$X\left(^{12}CH_2D_2\right)_{stochastic} = 6X\left(^{12}C\right)X(H)^2X(D)^2. \quad (9)$$

The relationship between $\Delta^{13}CH_3D$, $\Delta^{12}CH_2D_2$, and temperature (Liu and Liu, 2016; Ma et al., 2008; Webb and Miller III, 2014) provides a useful reference curve in $\Delta^{13}CH_3D$ vs. $\Delta^{12}CH_2D_2$ space that depicts thermodynamic equilibrium (Young et al., 2017). Sample measurements plotted on the equilibrium curve are evidently in thermodynamic equilibrium. However, most methane gas samples lie off the curve, with isotopologue abundances reflecting kinetic effects (Ash et al., 2019; Giunta et al., 2021, 2019; Labidi et al., 2020; Young et al., 2017; Young, 2019). The $\Delta^{13}CH_3D$ and $\Delta^{12}CH_2D_2$ values for methane produced by the microbial methanogenesis incubations should be largely independent of substrate effects and are distinctive, with $\Delta^{13}CH_3D \sim +2.5$ to $-4.0‰$ and $\Delta^{12}CH_2D_2 \sim -20$ to $-45‰$, respectively. These negative values have been attributed to either a "combinatorial" effect in the case of $\Delta^{12}CH_2D_2$ (Taenzer et al., 2020) or classical and/or quantum kinetic effects that could affect both values (Young et al., 2017).

Here, we are concerned with the effects of aerobic oxidation of methane on $\Delta^{13}CH_3D$ and $\Delta^{12}CH_2D_2$ values in methane gases and how these effects might be observable in natural settings. Recognition of the effects of oxidation may be critical to using $\Delta^{13}CH_3D$ and $\Delta^{12}CH_2D_2$ values as tracers of the provenance of methane gases.

Methylosinus trichosporium (OB3b) is a obligate aerobic methanotrophic bacterium belonging to the alpha proteobacteria class that oxidizes methane to CO_2 according to Equation (1) (Hanson and Hanson, 1996). It is one of few aerobic methanotrophs with both soluble and particulate methane monooxygenase, which are the main enzymes that facilitate the oxidation of methane (Hanson and Hanson, 1996; Murrell, 2010). *M. trichosporium* is one of the best characterized aerobic methanotrophic bacterium and an excellent candidate for isotope studies because it has been studied

in a wide variety of environments and in pure cultures (Murrell, 2010). However, methane isotopologue signatures of *M. trichosporium* consuming methane sources are non-existent.

2. Previous work

Wang et al. (2016), the only other study on the effect of MOx on methane isotopologue signatures we are aware of, investigated pure cultures of *Methylococcus capsulatus* (Bath), in liquid medium, at two temperatures in the presence of methane and oxygen. The abundances of head-space methane isotopologues, including $^{12}CH_4$, $^{13}CH_4$, $^{12}CH_3D$ and $^{13}CH_3D$ were measured over time while methane was consumed with oxygen. Methane carbon ($^{13}C/^{12}C$) and hydrogen (D/H) isotope ratios became progressively higher with time, consistent with a classical kinetic isotope effect, in which isotopically light methane was preferentially oxidized by the aerobic methane-oxidizing bacteria. The $\Delta^{13}CH_3D$ signatures became progressively lower in both temperature incubations, a trend that is also consistent with classical kinetic effects. These measurements allowed Wang et al. to calculate fractionation factors (α) for $^{13}CH_4$, $^{12}CH_3D$ and $^{13}CH_3D$ relative to $^{12}CH_4$, where the fractionation factors are defined as, for example, $\alpha_{13CH3D} = (^{13}CH_3D/^{12}CH_4)/(^{13}CH_3D/^{12}CH_4)_o$ where the subscript zero signifies the ratio prior to reaction. The study introduced the gamma factor (γ) to describe deviations from the Rule of the Geometric Mean, or RGM (Bigeleisen, 1955). The RGM articulates the zero-order expectation that the fractionation factor for a multiply-substituted isotopologue will be approximately equal to the product of the fractionation factors for the constituent singly-substituted species. For example, one might predict that the fractionation factor for $^{13}CH_3D/^{12}CH_4$ would be the product of the fractionation factor for $^{13}CH_4/^{12}CH_4$ and that for $^{12}CH_3D/^{12}CH_4$, i.e., $\alpha_{13CH3D} = \alpha_{13CH4}\ \alpha_{12CH3D}$. By defining the γ parameters as the ratio of observed α to the α predicted by the RGM (Equations (10) and (11)), the deviations from this simple expectation are quantified; if γ is equal to 1 then the mass-18 isotopologue fractionation is ideal in that it follows the expectations from the RGM:

$$^{13D}\gamma = \frac{^{13D}\alpha}{^{13}\alpha \cdot {}^{D}\alpha} \tag{10}$$

$$^{D2}\gamma = \frac{^{D2}\alpha}{^{D}\alpha \cdot {}^{D}\alpha} \tag{11}$$

Deviations from the RGM imply complexities involving the isotopes of interest due to the "clumping" of the heavy isotopes on bonds. Wang et al. applied their γ's and α's to a simple open system model attributed to Hayes (2001), which depicts a flow system where methane flows through the system as it is removed by oxidation. Steady state in this case is achieved because of a constant flux into the system, a constant reaction rate, and a constant flux out of the system.

Using this simple calculation, the authors demonstrated that the degree, and even the sign, of fractionation of $\Delta^{13}CH_3D$ is critically sensitive to γ, with deviations from unity by a factor ± 0.002 resulting in differences in $\Delta^{13}CH_3D$ of several per mil with progressive oxidation. Although Wang et al. (2016) was the first study to obtain $\Delta^{13}CH_3D$ signatures from MOx, the α and γ factor for the $\Delta^{12}CH_2D_2$ were not obtained.

Haghnegahdar et al. (2017) used ab initio calculations to calculate fractionation factors for $\Delta^{13}CH_3D$ and $\Delta^{12}CH_2D_2$ associated with abiotic oxidation of methane by hydroxyl and chlorine radicals in the atmosphere. They found that at steady state, atmospheric CH_4 should have exceptionally high $\Delta^{12}CH_2D_2$ values of order +100 ‰ relative to the sources because of relatively low γ values for this species. They concluded that $\Delta^{12}CH_2D_2$ values may prove to be sensitive tracers of methane sources and sinks in the atmosphere (Haghnegahdar et al., 2017). Such strikingly positive $\Delta^{12}CH_2D_2$ values that contrast with expectations from simple kinetics, and result from deviations in γ values from unity, underscore the need to characterize the effects of oxidation on $\Delta^{13}CH_3D$ and $\Delta^{12}CH_2D_2$. Ab initio calculations for microbially-mediated oxidation are challenging. However, laboratory experiments provide a more direct means of assessing these effects.

Fig. 1. Three-liter glass flange flask containing *Methylosinus trichosporium* colonies on NMS agar plates. Agar plates are placed into shelves of a custom-built stainless-steel rack. Close up picture shows example of *M. trichosporium* colonies on an agar plate.

In the present study we use pure cultures of *Methylosinus trichosporium* (OB3b) to characterize the isotopologue effects of methane consumption during MOx. Our goals are four-fold: 1) observe the $\Delta^{13}CH_3D$ and $\Delta^{12}CH_2D_2$ signatures from MOx in closed system pure culture experiments; 2) calculate α's and the γ's that affect $\Delta^{13}CH_3D$ and $\Delta^{12}CH_2D_2$ values due to MOx operating in closed systems; 3) apply the derived α's and γ's to determine the trajectories of oxidation in $\Delta^{13}CH_3D$ vs. $\Delta^{12}CH_2D_2$ space for Rayleigh distillation in closed systems, production and oxidation in closed systems leading to a steady state, and oxidation where methane flows through systems and 4) characterize the effects of oxidation in terms of the resulting trajectories in mass-18 methane isotopologue space.

3. Materials and methods

3.1. Pure culture cultivation

Cells from a dense contamination-free culture of *Methylosinus trichosporium* (OB3b) in liquid Nitrate Mineral Salts medium

Table 1
Experimental details and methane isotopologues result from incubations of methane with Methylosinus trichosporium (OB3b).

Incubation Time (d)	Volume of gas analyzed (mL)	F $((CH_4/N_2)/(CH_4/N_2)_{initial})$	O_2/N_2 Area	$\delta^{13}C$ (1 se) (‰)	δD (1 se) (‰)	$\delta^{13}CH_3D$ (1 se) (‰)	$\Delta^{13}CH_3D$ (1 se) (‰)	$\delta^{12}CH_2D_2$ (1 se) (‰)	$\Delta^{12}CH_2D_2$ (1 se) (‰)
0	10	1.000	0.2377	−39.93 (0.006)	−147.79 (0.038)	−95.28 (0.19)	2.27 (0.22)	−173.88 (0.83)	6.11 (1.00)
12	10	0.5168	0.0152	−30.11 (0.004)	21.37 (0.028)	94.11 (0.16)	1.10 (0.15)	172.17 (0.89)	−6.14 (0.77)
15	10	0.5196	0.0014	−30.07 (0.006)	21.31 (0.029)	94.09 (0.16)	1.10 (0.15)	174.23 (1.15)	−4.28 (0.98)
30	15	0.5156	0.0145	−30.37 (0.014)	21.04 (0.020)	93.84 (0.43)	1.46 (0.40)	171.81 (0.65)	−5.79 (0.56)
0	10	1.000	0.2725	−37.41 (0.004)	−145.01 (0.021)	−89.22 (0.12)	3.08 (0.13)	−168.24 (0.58)	6.42 (0.70)
1	10	0.9688	0.2147	−36.47 (0.006)	−123.23 (0.021)	−65.81 (0.12)	2.33 (0.13)	−124.69 (0.67)	7.14 (0.76)
3	10	0.7356	0.1165	−34.59 (0.005)	−76.74 (0.025)	−14.71 (0.19)	1.97 (0.20)	−32.53 (0.86)	3.90 (0.89)
4	10	0.6733	0.078	−33.29 (0.005)	−51.79 (0.022)	12.97 (0.18)	1.67 (0.18)	19.06 (0.61)	2.53 (0.60)
7	15	0.6114	0.017	−31.22 (0.004)	−3.17 (0.021)	66.16 (0.13)	0.70 (0.12)	117.41 (0.75)	−5.35 (0.67)
9	15	0.5701	0.0144	−31.15 (0.004)	−2.14 (0.023)	68.10 (0.13)	1.40 (0.12)	118.25 (0.74)	−6.65 (0.67)

(NMS) were transferred to an NMS agar in sterile petri dishes (Fig. 1). Prior to inoculation, NMS agar was prepared with basal salts containing 0.93 g/L $MgSO_4 \bullet 6\ H_2O$, 10 g/L KNO_3, 1.22 g/L $CaCl_2$, 0.15 ml/L of 1 M PO_4 solution, 5 ml/L of 2 M HEPES buffer and 15 g/L agarose modified from Whittenbury et al. (1970). One ml/L trace element solution and 1 ml/L vitamin solution according to Widdel and Pfennig (1981) was added to the NMS agar medium. The medium was autoclaved, and pH was adjusted to 7. While medium was dispensed to the petri dishes, 5 mL of Cycloheximide (1%) was added to the NMS agar to avoid contamination by fungal eukaryotes. In a sterile (UVC light sterilization) clean bench (VWR PCR workstation Pro HEPA), equipped with a HEPA filter for providing germfree airflow, a total of 6 NMS agar plates were inoculated with the culture of *M. trichosporium* (OB3b) by dipping a sterile metal culture loop into the liquid culture and then spreading the loop over the surface of the NMS agar plate. The inoculated plates were then placed without lids into the shelves of a custom made sterile stainless-steel rack (Fig. 1). While still in the clean bench, the stainless-steel rack with inoculated NMS agar plates was carefully placed into a sterile 3-liter glass flange flask (Glasgerätebau Ochs, Germany), and closed air-tight (via an O-ring connection and quick release clamp) at atmospheric pressure with a glass flange lid equipped with four butyl stopper-sealed openings (one GL 45, one GL 25, and two N20) (Fig. 1). Outside the clean bench, 1.2 liters of Ultra-high pure methane (Airgas) was injected into the sealed flange flask through the butyl rubber stopper in one of the N20 openings using a sterile 60 mL plastic syringe equipped with a 0.2 µm syringe sterile filter and a needle, raising the internal pressure by ∼1.4 times atmospheric pressure. The headspace was then mixed by repetitive plunging of the 60 mL plastic syringe >10 times to ensure that the air and methane were properly mixed. The sealed flange flask with inoculated agar plates was stored in the dark at room temperature for incubation.

3.2. Incubation parameters

We conducted two time series incubations at room temperature with the same *M. trichosporium* (OB3b) inoculum inside the flange flask as described in section 3.1. The first time series lasted a total of 30 days, during which the headspace was sampled at 0, 12, 15, and 30 days (Table 1). The second time-series lasted a total of 9 days, where methane headspace was sampled at 0, 1, 3, 4, 7 and 9 days (Table 1). The second incubation provided a higher temporal resolution during the first nine days after methane addition. Between incubations, the headspace in the glass flange flask was completely exchanged by opening the flange flask inside the clean bench and flushing with HEPA-filtered air for 30 min. After flushing, the flange flask was sealed and supplied with new methane gas (see section 3.1). Over the course of both incubations, the *M. trichosporium* (OB3b) inoculum developed rich, macroscopic colonies on the NMS agar (Fig. 1).

3.3. Methane isotopologue measurements

3.3.1. Headspace subsampling and methane purification

Abundances of the singly and doubly-substituted methane isotopologues $^{12}CH_4$, $^{13}CH_4$, $^{12}CH_3D$, $^{13}CH_3D$ and $^{12}CH_2D_2$ in this study were measured on the Panorama mass spectrometer (Nu Instruments) located at the University of California, Los Angeles. Prior to mass spectrometric measurements, the headspace of the glass flange flask containing the *M. trichosporium* colonies was subsampled at each time point (see 3.1) by inserting the needle of a 5 mL gas-tight glass syringe through a butyl rubber stopper in one of the N20 openings. Total subsample volumes for each time point can be found in Table 1. Subsample volumes were aliquoted into 5 mL portions, until the 60-100 µmol CH_4 threshold required for methane analyses on the Panorama mass spectrometer was met. The methane fraction within the subsampled gas was purified from the remaining air fraction according to methods described by Young et al. (2017). Briefly, the gas aliquots were injected into a vacuum line interfaced to a gas chromatograph. Water vapor and carbon dioxide were separated from the gas sample in a liquid nitrogen trap for 10 mins. The remaining gas sample was then captured by freezing methane onto silica gel within a second trap with liquid nitrogen for 30 mins. The frozen silica gel trap was then flushed with helium gas and then warmed to ∼40°C to transfer the sample to the GC. Methane was purified using two GC columns in series. The first is a 5 A molecular sieve packed column used to separate oxygen and nitrogen from CH_4. The second is a packed HayeSep D column used to separate methane from other hydrocarbons in the gas sample. A passive thermal conductivity detector (TCD) was used to identify peaks. The area of peaks for oxygen, nitrogen and methane were recorded. Retention time of methane gas was approximately 17 minutes with a carrier He flow rate of 20 ml/minute.

Upon exiting the TCD, the purified methane was captured by freezing a trap filled with silica gel with liquid nitrogen for 30 mins. After collection, helium was pumped away, and the frozen silica gel with methane was then heated (∼40°C) and the effusing methane was captured in a separate glass vial filled with silica gel at liquid nitrogen temperature for 30 mins. The sealed glass vial with the purified methane was removed from the vacuum line and attached to the dual inlet located on the mass spectrometer where it was then concentrated into a “cold finger” filled with silica gel

at liquid nitrogen temperature. The gas was then released to the variable volume of the dual inlet of the instrument by heating the silica gel to 30°C

3.3.2. Mass spectrometer measurements

The Panorama instrument is described by Young et al. (2016). Briefly, the instrument operates at a mass resolving power ($m/\Delta m$) of ~ 40,000, which enables measurements of $^{12}CH_4^+$, $^{13}CH_4^+$, $^{12}CH_3D^+$, $^{13}CH_3D^+$, and $^{12}CH_2D_2^+$ ion currents in the same gas sample with no significant mass interferences. The abundances of both $^{13}CH_3D$ and $^{12}CH_2D_2$ are measured using an electron multiplier. Measurements were made with two magnet mass settings. The magnet was first adjusted to measure $^{12}CH_2D_2^+$ (18.04385 amu) in the ion counter. The $^{12}CH_2D_2^+/^{12}CH_4^+$ and $^{12}CH_3D^+/^{12}CH_4^+$ ratios were used to determine the $\Delta^{12}CH_2D_2$ and δD values, where $\delta D = 10^3(^DR/^DR_{VSMOW}\text{-}1)$, ^DR is the D/H ratio, and VSMOW refers to the international reference value. Measurements of these ratios consisted of 40 blocks of alternating sample/standard measurements of 30 s each. The ratios $^{13}CH_4^+/^{12}CH_4^+$ and $^{13}CH_3D^+/^{12}CH_4^+$ in the same gas sample were obtained with the magnet set at 18.04090 amu for the axial collector. Twenty blocks were obtained for these measurements. These ratios combined with those from the previous mass setting were used to calculate $\Delta^{13}CH_3D$ and $\delta^{13}C$ values, where $\delta^{13}C = 10^3(^{13}R/^{13}R_{PDB}\text{-}1)$, ^{13}R is the $^{13}C/^{12}C$ ratio, and PDB refers to the international reference value. Typical external reproducibility as determined by multiple measurements of shale gas for δD, $\Delta^{12}CH_2D_2$, $\delta^{13}C$ and $\Delta^{13}CH_3D$ are 0.2, 0.6, 0.1, and 0.2 ‰, respectively, at the 1σ level, based on replicate samples (Young et al., 2017). We also report $\delta^{13}CH_3D$ and $\delta^{12}CH_2D_2$ values relative to the laboratory reference gas for purposes of extracting fractionation factors.

3.4. Determination of fractionation factors and gamma's

A key objective of this study was to determine fractionation factors (α) for the $^{13}CH_4$, $^{12}CH_3D$, $^{13}CH_3D$ and $^{12}CH_2D_2$ isotopologues relative to $^{12}CH_4$ during the MOx incubations. For this purpose, we made use of the Rayleigh fractionation equation that describes the isotopologue effects of uptake of methane from a well-mixed reservoir of gas.

To obtain the α values from our data, isotope ratios relative to the reference materials were obtained from delta values obtained by mass spectrometry using

$$\frac{R}{R_{std}} = \frac{\delta}{1000} + 1, \tag{12}$$

where R represents the isotope ratio of interest and subscript *std* is the standard used as the reference for the deltas. The ratio in Eq. (12) taken at time t was then divided by the same ratio at the time zero to then obtain a measure of the change in ratio with time:

$$\frac{\frac{R^t}{R_{std}}}{\frac{R^0}{R_{std}}} = \frac{R^t}{R^0} \tag{13}$$

This ratio in turn can be used in the Rayleigh equation for fractionation from a well-mixed reservoir, in our case the methane comprising the head-space gas, using

$$\frac{\frac{\delta}{1000}+1}{\frac{\delta^0}{1000}+1} = \left(\frac{^{12}CH_4}{^{12}CH_4^o}\right)^{\alpha-1}, \tag{14}$$

where α is the fractionation factor for the methane isotopologues, and $^{12}CH_4/^{12}CH_4^o$ is the fraction of methane remaining in the head space, often referred to as F (and closely approximated by the ratio of the major isotopologues to the initial value).

Applying the natural logarithm of both sides in Eq. (14), we have

$$ln\left(\frac{R}{R^0}\right) = (1-\alpha)\,(-lnF)\,. \tag{15}$$

The form of Equation (15) is useful as the slope for $\ln(R/R^o)$ vs. $-\ln(F)$ yields the fractionation factors, α, we seek. The ratios of methane to nitrogen GC areas were used to obtain values for F. Standard error propagation (with 1σ error) was used (York et al., 2004) to propagate errors in both $\ln(R/R^o)$ from the isotope ratio measurements themselves, and in $-\ln(F)$ to uncertainties in the derived fractionation factors (from errors in the regression slopes). Uncertainties in $-\ln(F)$ were obtained by replicate (n=5) samplings of head-space gas in the absence of microbes, indicating methane concentration errors of 0.3% of the measured value.

4. Results

4.1. Methane isotopologue trends with time

Throughout the two-time series in this study, large cell colonies were visible on the NMS agar plates (Fig. 1). We observed buildup of water condensation on the walls of the glass flange flask and gas chromatography showed lower methane and oxygen concentrations with longer incubation periods (Table 1). By the 12th day of the first long incubations the fraction of methane remaining in the chamber (F) was ~0.52 and showed no further decrease up to day 30. In the second, shorter incubation, the fraction of methane (F) remaining was ~0.57 by day 9 (Table 1). We note that the measurement taken at day 7 was negatively affected by a software error in peak areas. A correction for the F value of the 7th day was calculated using the F values from the 4th and 9th days of the short incubation.

The initial bulk isotopic compositions for the long and short incubations were −39.93‰ and −37.41‰ for $\delta^{13}C$ and, −147.79‰ and −145.01‰ for δD, respectively. With time, the $\delta^{13}C$ and δD values for the headspace methane became less negative in both time series. In the longer-duration incubation the methane $\delta^{13}C$ increased from −39.93‰ to −30.37‰ and the δD increased from −147.79‰ to 21.04‰ after 30 days (Table 1). In the shorter-duration incubation the $\delta^{13}C$ increased from −37.41‰ to −31.15‰ and δD increased from −145.01‰ to −2.14‰ after 9 days (Table 1). The initial mass-18 compositions on day 0 for the long and short incubations were 2.27‰ and 3.08‰ for $\Delta^{13}CH_3D$ and 6.11‰ and 6.42‰ for $\Delta^{12}CH_2D_2$, respectively. There was a 0.8‰ difference in $\Delta^{13}CH_3D$ and a 0.3‰ difference in $\Delta^{12}CH_2D_2$ between starting compositions in each incubation, evidently from the result of analytical uncertainties and/or small fractionations imparted by the gas loading procedure. The $\Delta^{13}CH_3D$ and $\Delta^{12}CH_2D_2$ values in both incubations became more negative as the incubations progressed. In the longer incubation, the $\Delta^{13}CH_3D$ decreased from 2.27‰ to 1.46‰ while $\Delta^{12}CH_2D_2$ decreased from 6.11‰ to −5.79‰ after 30 days (Table 1). In the shorter incubation, the $\Delta^{13}CH_3D$ values decreased from 3.08‰ to 1.40‰ while $\Delta^{12}CH_2D_2$ decreased from 6.42‰ to −6.65‰ after 9 days (Table 1).

4.2. Isotopologue fractionation factors departures from the RGM

Fig. 2 shows the slopes defined by $1000\ln(R/R_o)$ and $-\ln(F)$ and the corresponding α values for the four methane isotopologues relative to $^{12}CH_4$. The derived slopes are 15.15 ± 0.06 for $^{13}C/^{12}C$, 273.5 ± 1.0 for D/H, 285.9 ± 1.1 for $^{13}CH_3D/^{12}CH_4$,

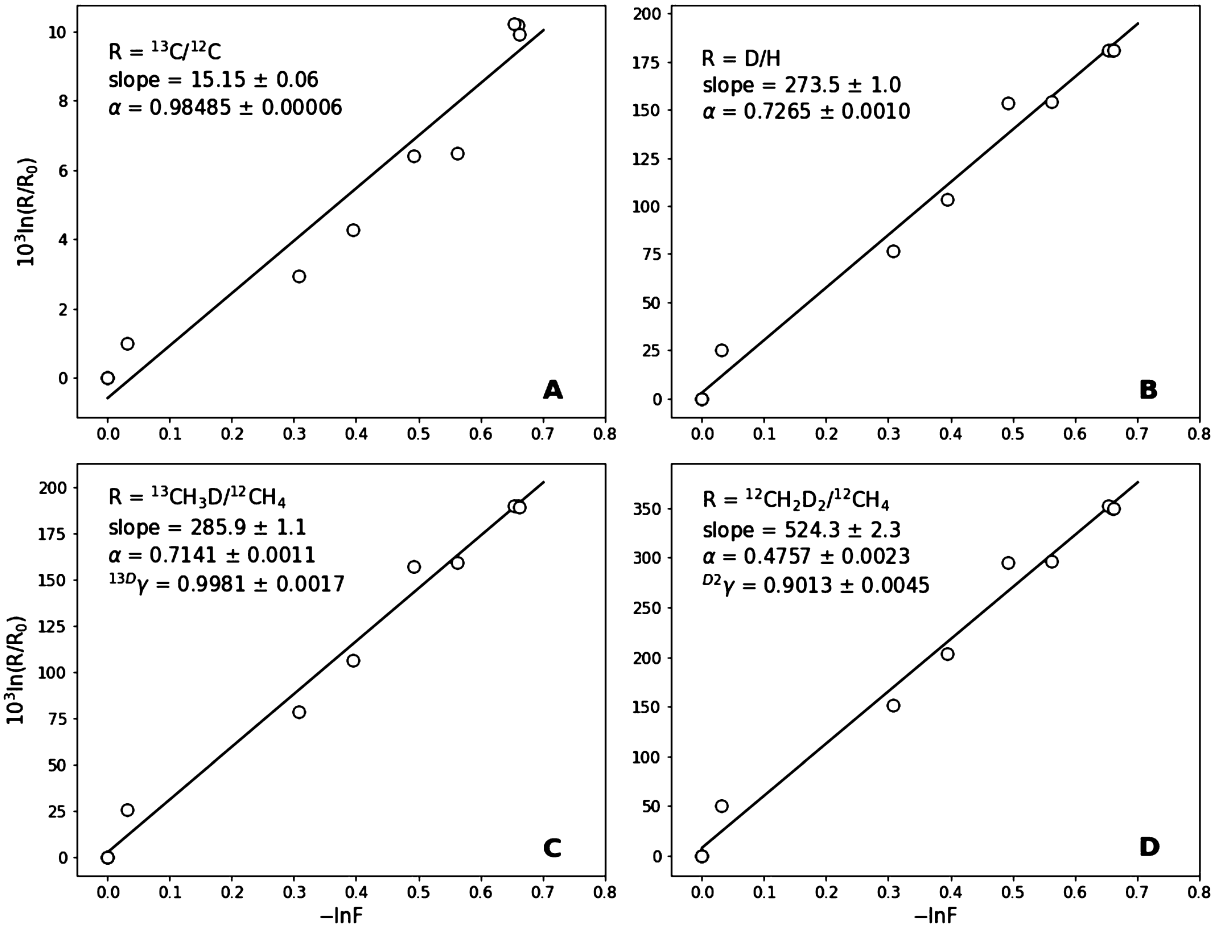

Fig. 2. Derived fractionation factors (α's) and mass-18 isotopologue γ's (C and D) from linear regressions of MOx experimental data assuming Rayleigh fractionation for carbon (A), hydrogen (B), $\Delta^{13}CH_3D$ (C) and $\Delta^{12}CH_2D_2$.

and 524.3 ± 2.3 for $^{12}CH_2D_2/^{12}CH_4$. The corresponding fractionation factors, α's, are 0.98485 ± 0.00006 for $^{13}C/^{12}C$, 0.7265 ± 0.0010 for D/H, 0.7141 ± 0.0011 for $^{13}CH_3D/^{12}CH_4$, and 0.4757 ± 0.0023 for $^{12}CH_2D_2/^{12}CH_4$. The γ values from these α values are 0.9981 ± 0.0017 and 0.9013 ± 0.0045 for $^{13}CH_3D/^{12}CH_4$, and $^{12}CH_2D_2/^{12}CH_4$, respectively.

5. Discussion

5.1. Fractionation of carbon, hydrogen, $^{13}CH_3D$ and $^{12}CH_2D_2$ during MOx

Higher bulk isotope ratios with progressive depletion of methane gas through uptake by a microbial community is expected in a closed system as a result of the kinetic advantages of the lighter species. Our derived fractionation factors can be used to calculate the enrichment factors for carbon and hydrogen, ε, where $\varepsilon = (\alpha - 1)1000$ for the species of interest. The resulting ε_C and ε_D in our study are -15.15 ± 0.06‰ and -273.5 ± 1.0‰, respectively. These MOx enrichment factors are within the range of those previously determined for MOx in laboratory pure and mixed cultures and environmental studies, where carbon enrichment factors range from (−3‰ to −38‰) and hydrogen enrichment factors (−38‰ to −320‰) (Barker and Fritz, 1981; Coleman et al., 1981; Feisthauer et al., 2011; Kinnaman et al., 2007; Templeton et al., 2006; Wang et al., 2016)

The calculated γ values, with 1σ error, for $^{13}CH_3D/^{12}CH_4$ using the average $^{13}C/^{12}C$ and D/H α's from both incubations of 0.9981 (± 0.0017) could be considered "ideal", in that fractionation is within error of the RGM. In other words, the fractionation of $^{13}CH_3D$ relative to $^{12}CH_4$ is approximately the product of the fractionation factors for bulk carbon and hydrogen isotopes. This result is consistent with the $^{13}CH_3D$ γ's calculated by Wang et al. (2016) who reported weighted averages $^{13}CH_3D$ γ's of 1.0005 (± 0.0003) and 1.0000 (± 0.0007) in their 30 and 37 °C incubations, respectively.

To the best of our knowledge, we here report the first $\Delta^{12}CH_2D_2$ values of methane involved in MOx, obtained from pure bacterial cultures. Unlike the "ideal" $^{13}CH_3D$ γ values, the $^{12}CH_2D_2$ γ values, with 1σ error, are distinctly lower than ideal, with a value of 0.9013 (± 0.0045) (Fig. 2), showing that the $^{12}CH_2D_2$ fractionation does not follow the RGM during MOx.

It is instructive to compare our MOx results to α's and γ's predicted for $^{12}CH_2D_2$ resulting from abiotic methane oxidation by hydroxyl radicals. The α's in our study for D/H and $^{12}CH_2D_2$ of 0.7265 (± 0.0010) and 0.4757 (± 0.0023), respectively, are similar to the fractionation factors for D/H and $^{12}CH_2D_2$, of 0.757 and 0.521 for OH oxidation of methane, respectively, obtained from ab initio calculations by Haghnegahdar et al. (2017). The value for the $^{12}CH_2D_2$ γ from our MOx pure culture experiments of 0.9013 ± 0.0045 is similar to the $^{12}CH_2D_2$ γ of 0.906 for oxidation by OH radicals implied by the results from e.g. Haghnegahdar et al. (2017).

The mechanism behind the low γ value for $^{12}CH_2D_2$ remains poorly understood. Ono et al. (2021), conducted experiments to elucidate the $\Delta^{13}CH_3D$ (not $\Delta^{12}CH_2D_2$) and singly-substituted isotopologue signatures during AOM and found the γ values for $^{13}CH_3D$ obtained in their study were unexpectedly lower than unity ($\gamma < 1$). In that work, the phenomenon was explained in

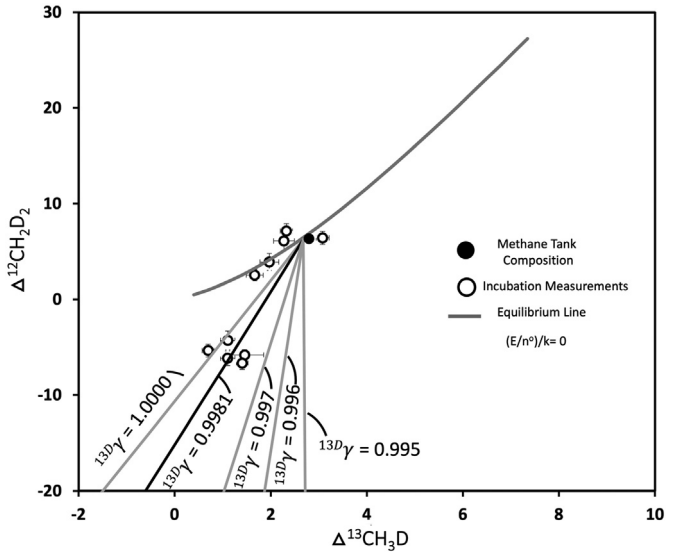

Fig. 3. Mass-18 isotopologue plot showing trajectories of residual methane gas affected by uptake by MOx in a closed system Rayleigh distillation model. Paths for different $^{13}CH_3D$ γ values at our measured γ for CH_2D_2 are shown. Solid black line is the trajectory using measured γ's from the MOx experiments in this study. Solid grey lines are modeled trajectories with a range of different $^{13}CH_3D$ γ's. Open circles are the MOx data from this study. The closed black circle is the starting methane isotopologue composition. The dark grey curve represents thermodynamic equilibrium for comparison.

terms of difference in zero-point energies from reactant-like to product-like transition states of the enzyme structure during the oxidation reaction. In this context, any solution involving zero-point energies will lead to larger effects where D substitutions for H are involved, as shown by the ab initio calculations by Haghnegahdar et al. (2017). In any case, it appears that deviations from RGM could indicate alteration of a methane source by oxidation. The transition states of the monooxygenase enzymatic in our study were not determined, and further research into the relationship of deviations of the RGM to enzyme transition state causing isotopologue effects should be conducted. Nevertheless, the low γ value for $^{12}CH_2D_2$ exerts a significant influence over the trajectories in mass-18 isotopologue space followed by methane affected by MOx, as discussed next.

5.2. Trajectories of $\Delta^{13}CH_3D$ and $\Delta^{12}CH_2D_2$ in open and closed systems

Our results allow us to characterize the trajectories followed by methane in $\Delta^{13}CH_3D$ vs. $\Delta^{12}CH_2D_2$ space as it is consumed by MOx in either open or closed systems. We find that these trajectories are controlled by the precise values for γ's. In order to illustrate the effects of γ's, we consider three cases, oxidation in the absence of production in a closed system (the case for our incubations), oxidation with production in closed systems, and the steady-state case where transport (flow) is balanced against oxidation.

5.2.1. Rayleigh distillation in closed systems

We first consider the closed system case where methane is consumed by a Rayleigh distillation process in which only aerobic oxidation of methane is occurring, and no new methane is being supplied to the system. Fig. 3 shows the calculated trajectories of residual methane gas in $\Delta^{13}CH_3D$ vs. $\Delta^{12}CH_2D_2$ space based on our measured MOx fractionation factors. The overall trend shows decreases in both $\Delta^{13}CH_3D$ and $\Delta^{12}CH_2D_2$. For comparison, we also show calculated trajectories in $\Delta^{13}CH_3D$ vs. $\Delta^{12}CH_2D_2$ space for a range in $^{13}CH_3D$ γ values at a fixed value for the $^{12}CH_2D_2$ γ that matches the value measured in our incubations (Fig. 3). Although the paths become steeper for $^{13}CH_3D$ γ less than 1, the paths are all similar in showing decreasing $\Delta^{12}CH_2D_2$ with more moderate changes in $\Delta^{13}CH_3D$ where only oxidation occurs (Fig. 3).

5.2.2. Time-dependent oxidation with production

Next we consider the case where there is a balance between methane production and consumption over time in a closed system (Haghnegahdar et al., 2017). Here, a constant rate of production is balanced against oxidation, where the oxidation is taken to be a first-order kinetic process with a fixed rate constant. The overall process is described by the ordinary differential equation,

$$\frac{dn_i}{dt} = E_i - k_i n_i, \tag{16}$$

where n_i is the time variant moles of the isotopologue of interest i, E_i is the methane source term for species i, and k_i is the rate constant for oxidation of i (yr^{-1}). The solution for the time-dependent variability in moles of isotopologue i is,

$$n_i(t) = n_i^o e^{-k_i t} + \frac{E_i}{k_i}\left(1 - e^{-k_i t}\right), \tag{17}$$

where n_i^o is the initial moles of i and t is time. The steady-state moles of the methane isotopologue species i are obtained by evaluating (17) where $t \to \infty$, and thus $e^{(-k_i t)} \to 0$, yielding

$$n_i\,(t \sim \infty) = \frac{E_i}{k_i}. \tag{18}$$

The steady-state amount of methane is thus seen to be controlled by the ratio of the methane production rate and the methane oxidation rate constant. The steady-state ratio of two isotopologues is then,

$$\frac{n_i\,(t \sim \infty)}{n_j\,(t \sim \infty)} = \frac{k_i E_j}{E_j k_i}, \tag{19}$$

where n_i (n_j) is the amount of moles of isotopologue i (j), E_i (E_j) is the methane source term for i (j), and k_i (k_j) is the rate constant for oxidation of i (j). Fig. 4 shows the calculated trajectories of methane gas in $\Delta^{13}CH_3D$ vs. $\Delta^{12}CH_2D_2$ space based on Equation (17) for $(E/n^o)/k$ of 1. We address the effects of different $(E/n^o)/k$ in greater detail below. Steady state will be achieved in several e-folding times for oxidation (i.e., where $t >> 1/k_i$). For the α and γ values measured in our experiments, the path followed by methane begins with moderate decreases in $\Delta^{13}CH_3D$ and $\Delta^{12}CH_2D_2$ followed by modest increases in $\Delta^{13}CH_3D$ and, eventually, dramatic increases in $\Delta^{12}CH_2D_2$ with progressive oxidation. The precise path, however, is exceedingly sensitive to the γ value for $^{13}CH_3D$ (Fig. 4). While $\Delta^{12}CH_2D_2$ always increases dramatically, when γ for $^{12}CH_2D_2$ is less than 1, and we assume this to be true in all cases, the magnitude, and even the sign of $\Delta^{13}CH_3D$ changes with even small differences in γ for $^{13}CH_3D$ of 0.001. Lowering the $^{13}CH_3D$ γ from 0.997 to 0.996, for example, is sufficient to cause a change in sign in the shift in $\Delta^{13}CH_3D$ with oxidation (Fig. 4).

5.2.3. Oxidation in open systems at steady state

Next, we consider the situation in which the supply of methane in the system is not from local biota, but from an outside flux of methane into the system, through the region of oxidation, after which methane exits again. The calculated α's from the experimental data were applied to an open system steady-state flow-through model (Hayes, 2001). We first rearrange the mass balance equation to obtain for the steady state case,

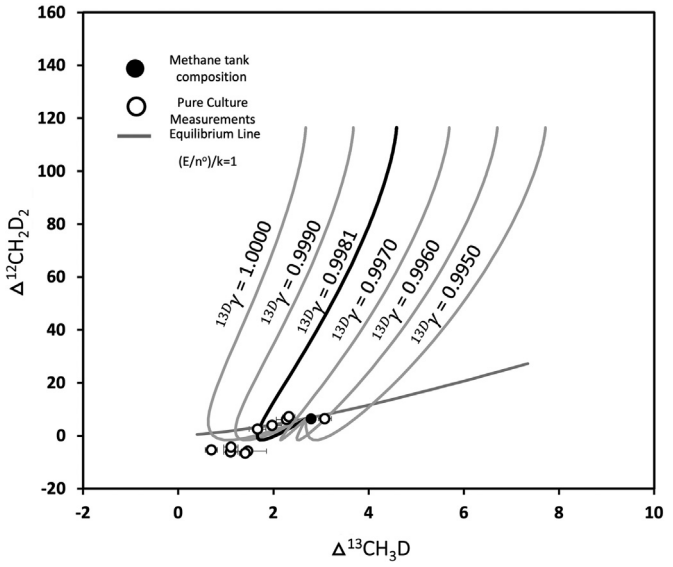

Fig. 4. Mass-18 isotopologue plot showing trajectories of the mass-18 isotopologues in a closed-system time dependent model (e.g., Haghnegahdar et al., 2017) when production and oxidation rate constants are equivalent ((E/n°)/k =1) and with varying $^{13}CH_3D$ γ. Solid black line is the trajectory using our measured γ's from the MOx experiments. Solid grey lines are modeled trajectories with varying $^{13}CH_3D$ γ's. Open circles are experimental data points to demonstrate the difference in mass-18 isotopologue signatures in our experiments to the mass-18 trajectories in the open system flow-through model. The closed black circle is the starting methane isotopologue composition to compare with the experimental data points and the mass-18 trajectories in the open flow-through system. The dark grey curved line is the thermodynamic equilibrium curve for reference.

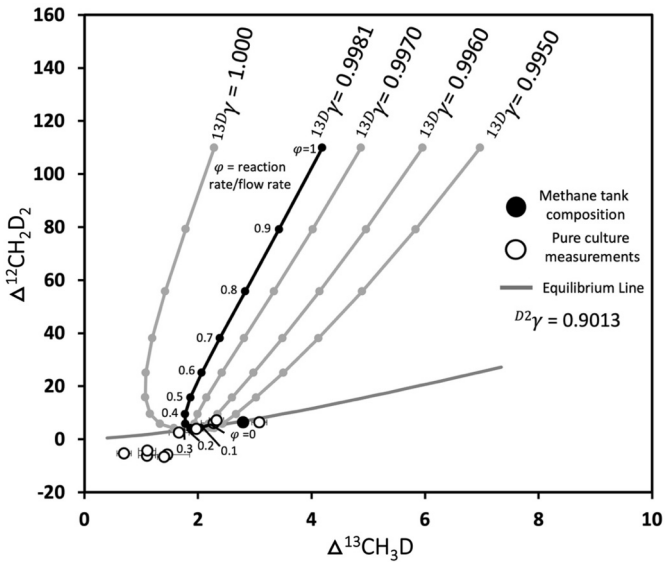

Fig. 5. Mass-18 isotopologue plot showing different steady-state methane compositions in an open flow- through system from Hayes (2001), with varying $^{13}CH_3D$ γ. The circles on the curves represent the steady state values for different relative rates of flow and oxidation (φ, see text). Solid black line is the trajectory defined by different steady-state values using the measured γ's from the MOx experiments. Solid grey lines are modeled trajectories with varying $^{13}CH_3D$ γ's. Open circles are experimental data points to demonstrate the difference in mass-18 isotopologue signatures in our experiments to the mass-18 trajectories in the open system flow-through model. The closed black circle is the starting methane isotopologue composition to compare with the experimental data points and the mass-18 trajectories in the open flow-through system. The dark grey curved line is the thermodynamic equilibrium line.

$$R^o = (1-\varphi)\,R + R\varphi\alpha, \tag{20}$$

where R^o is the initial isotopologue ratio, R is the steady state value, φ is the ratio of methane oxidation rate to residence time of the gas in the flow system, and α is the fractionation factor for the MOx reaction. Substitution of $\delta + 1$ for R yields the equation cited by Wang et al. (2016),

$$\delta = \frac{\delta^o + 1}{1 + \varphi(\alpha - 1)} - 1. \tag{21}$$

Fig. 5 shows calculated $\Delta^{13}CH_3D$ and $\Delta^{12}CH_2D_2$ values in the steady-state flow-through open system scenario. Each point along the curve represents a steady state at different values for φ. While resembling the curves in Fig. 5, these curves do not depict time evolution, but rather a series of possible steady-state compositions for methane affected by oxidation in the presence of flowing gas. The parameter φ in Equation (20) is a normalized version of the Dahmköhler number, Da, where Da $= \tau/(1/k)$, τ is the residence time of gas in the system and k is the rate constant for the reaction. Therefore, φ = Da/(1+Da). When k is large in comparison to τ, Da is large and φ goes to its maximum value of unity and the situation approaches that in the last section where production is low compared with the rate of oxidation. Conversely, if k is lower than τ, φ goes to 0 and the methane in the system is unaffected by oxidation. Here again, the curves for cases in between are sensitive to small changes in γ for $^{13}CH_3D$. In all cases, the evolution of both $\Delta^{13}CH_3D$ and $\Delta^{12}CH_2D_2$ trajectories are above the thermodynamic equilibrium line when methane oxidation is dominant.

5.3. Implications

The analysis above shows that in a closed system, in the absence of introduction of fresh methane, oxidation will lower $\Delta^{12}CH_2D_2$ in the residual gas as oxidation progresses, and $\Delta^{13}CH_3D$ will decrease, stay the same, or even increase depending upon the precise γ values for $^{13}CH_3D$. In our analysis, we observe that $\Delta^{12}CH_2D_2$ is far removed from the RGM, and thus we have assumed that γ is always smaller than 1 for $\Delta^{12}CH_2D_2$ and that this is a robust feature of oxidation in all cases.

Where oxidation is balanced against production of methane, either in closed or open systems, one expects to find decreases in $\Delta^{12}CH_2D_2$ in the residual gas relative to the source where replenishment of the gas is negligible, but for production rates that are significant compared with rates of oxidation, the effect of oxidation is to raise $\Delta^{12}CH_2D_2$ values rather than lower them. This is a direct reflection of $^{12}CH_2D_2$ γ being smaller than 1. This proves to be a critically important observation for using mass-18 isotopologues as a means for determining the provenance and history of methane gases.

Recent work has determined the mass-18 isotopologue signatures of microbiologically produced methane in vitro and in vivo and the results suggest that $\Delta^{13}CH_3D$ and $\Delta^{12}CH_2D_2$ are markedly negative where methane is produced by microbial methanogenesis (e.g., -4 ‰ for $\Delta^{13}CH_3D$ and -43‰ for $\Delta^{12}CH_2D_2$) (Young et al., 2017). The question arises as to whether or not oxidation could mimic these mass-18 isotopologue signatures, thus adding confusion as to the origin of methane with low $\Delta^{12}CH_2D_2$ and low $\Delta^{13}CH_3D$ values. Our results suggest that in the absence of methane production, extreme degrees of oxidation (where a large fraction of the methane is consumed) could lead to low $\Delta^{12}CH_2D_2$ and $\Delta^{13}CH_3D$ values that might be confused with the signature of microbial methanogenesis. However, where production is simultaneous with oxidation, either in-situ (Fig. 4) or outside the region of oxidation where gas flows through the oxidation region (Fig. 5), the resulting $\Delta^{12}CH_2D_2$ and $\Delta^{13}CH_3D$ values do not resemble those produced by microbial methanogenesis (Fig. 6).

The precise positions of the gases in mass-18 isotopologue space will depend on the source, but if the source is microbial methanogenesis, then the residual gas will have either low

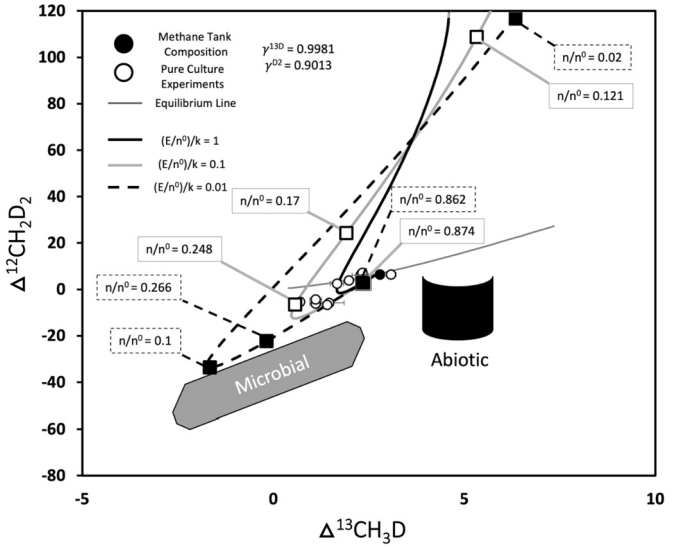

Fig. 6. Mass-18 isotopologue plot showing trajectories of the mass-18 isotopologues in a closed-system time dependent model (e.g., Haghnegahdar et al., 2017), with varying $(E/n^0)/k$. Solid black line is the trajectory using our measured γ's from the MOx experiments where $(E/n^0)/k = 1$. The solid grey line is the modeled trajectory using the measured γ's from the MOx experiments when $(E/n^0)/k = 0.1$. The dashed black line corresponds to the measured γ's from the MOx experiments where $(E/n^0)/k = 0.01$. Open and closed squares represent the mole ratio as time proceeds when $(E/n^0)/k$ equals 0.1 and 0.01, respectively. Open circles are experimental data points from this study. The closed black circle is the starting methane isotopologue composition. The dark grey curved line is the thermodynamic equilibrium curve for reference. Grey solid polygon represents the microbial field. Black solid cylinder represents the abiotic field.

$\Delta^{12}CH_2D_2$ (and $\Delta^{13}CH_3D$) or higher values with oxidation where the source persists. Indeed, the confusion that may arise where methane is added to a region of methane oxidation is that the microbial source of methane might be less evident because the $\Delta^{12}CH_2D_2$ values will be higher than expected.

From the preceding analysis it is clear that the ratio of production rate to consumption rate will influence the trajectory of residual methane during aerobic oxidation of methane. We illustrate the impact of varying rate constants of methane production relative to methane oxidation $(E/n^0)/k$ in the Fig. 6. Lowering $(E/n^0)/k$ to $<<1$ forces the $\Delta^{12}CH_2D_2$ and $\Delta^{13}CH_3D$ trajectory of the residual methane into the microbial methanogenesis field where more than 90% of the methane has been consumed (Fig. 6). Further oxidation results in an increase in $\Delta^{12}CH_2D_2$ above the thermodynamic equilibrium line as the residual methane is consumed by oxidation, but the fraction of methane remaining is exceedingly small by this stage (Fig. 6). We note that trajectories of residual methane in $\Delta^{12}CH_2D_2$ vs. $\Delta^{13}CH_3D$ space are almost indistinguishable for $(E/n^0)/k$ of 1, 10, 100, and 1000 (not shown). This finding illustrates explicitly that only where replenishment of methane is very low can MOx mimic microbial production in $\Delta^{12}CH_2D_2$ and $\Delta^{13}CH_3D$ space.

With this result in hand, we can return to the example of the methane in the Oman Ophiolite. We conclude that the low $\Delta^{12}CH_2D_2$ and $\Delta^{13}CH_3D$ values exhibited by some of the gas emanating from the ultramafic complex reported in Nothaft et al. (2021) are best interpreted as a microbial source of methane unless oxidation was acting on existing gas in the absence of any source of methane. The latter seems unlikely, bolstering the use of these mass-18 isotopologues as tracers of microbial methanogenesis.

6. Conclusions

In the present study we observed the $\Delta^{12}CH_2D_2$ and $\Delta^{13}CH_3D$ signatures over time in a closed system chamber containing aerobic methane-oxidizing bacteria in pure cultures. The results were used to obtain α's and γ's for both $\Delta^{12}CH_2D_2$ and $\Delta^{13}CH_3D$. We conclude that MOx fractionates $^{13}CH_3D$ "ideally" with respect to RGM, which validates previous work. We report for the first time measured α's and γ's for $^{12}CH_2D_2$ from MOx (to the best of our knowledge). We conclude that the fractionation of $^{12}CH_2D_2$ exhibits marked departures from the RGM, which tends to drive residual methane to high $\Delta^{12}CH_2D_2$ values with progressive oxidation where a source of methane is present during oxidation. The trajectories of residual methane gases in $\Delta^{12}CH_2D_2$ vs. $\Delta^{13}CH_3D$ space are sensitive to small deviations in $^{13}CH_3D$ from the RGM. Our results indicate that in a closed system, where methane production is absent, or occurring at very low rates relative to oxidation, the mass-18 isotopologue signatures of residual methane could potentially mimic microbial methanogenesis signatures. However, in a closed system where methane production and oxidation are simultaneously occurring, the MOx mass-18 isotopologue signatures are not at risk of mimicking microbial methanogenesis. Furthermore, we show that in open systems, where methane production is balanced by oxidation and advection, oxidation results in a combination of $\Delta^{13}CH_3D$ and $\Delta^{12}CH_2D_2$ values distinct from microbial methanogenesis, suggesting methane oxidation in an open system is clearly distinguishable from gas produced by microbial methanogenesis.

CRediT authorship contribution statement

Sebastian J.E. Krause: Conceptualization, Data curation, Formal analysis, Investigation, Methodology, Visualization, Writing – original draft. **Jiarui Liu:** Data curation, Formal analysis, Investigation, Software, Validation, Writing – review & editing. **Edward D. Young:** Conceptualization, Data curation, Formal analysis, Funding acquisition, Methodology, Project administration, Resources, Supervision, Writing – review & editing. **Tina Treude:** Conceptualization, Funding acquisition, Methodology, Project administration, Resources, Supervision, Writing – review & editing.

Declaration of competing interest

The authors declare that they have no known competing financial interests or personal relationships that could have appeared to influence the work reported in this paper.

Acknowledgements

The authors would like to acknowledge S. Krause (GEOMAR) for providing bacterial cultures and cultivation consultation. We also acknowledge I. Bussmann (AWI) for her consultation on cultivation of bacterial colonies. We acknowledge H. Tang (UCLA) for Panorama Mass Spectrometer training, assistance, and consultation. We further acknowledge J. Li and X. Huang (UCLA) for assistance with bacterial cultivation and sample preparation for measurements. This work received financial support through the University of California, the National Science Foundation (NSF) (Award No.: 1852912), National Aeronautics and Space Administration (NASA) (Award No.: 80NSSC21K1529) and the Sloan Foundation: Deep Carbon Observatory Grant (Award No.: G-2018-11346 and G-2017-9815 to E.D.Y.).

References

Ash, J., Egger, M., Treude, T., Kohl, I., Cragg, B., Parkes, R.J., Slomp, C., Sherwood Lollar, B., Young, E.D., 2019. Exchange catalysis during anaerobic methanotrophy

revealed by 12CH2D2 and 13CH3D in methane. Geochem. Perspect. Lett. 10, 26–30.
Barker, J.F., Fritz, P., 1981. Carbon isotope fractionation during microbial methane oxidation. Nature 293, 289–291.
Bigeleisen, J., 1955. Statistical mechanics of isotopic systems with small quantum corrections. I. General considerations and the rule of the geometric mean. J. Chem. Phys. 23, 2264–2267.
Boetius, A., Wenzhöfer, F., 2013. Seafloor oxygen consumption fuelled by methane from cold seeps. Nat. Geosci. 6, 725–734.
Bouquet, A., Mousis, O., Waite, J.H., Picaud, S., 2015. Possible evidence for a methane source in Enceladus' ocean. Geophys. Res. Lett. 42, 1334–1339.
Claypool, G.E., Kaplan, I.R., 1974. The origin and distribution of methane in marine sediments. In: Kaplan, I., Isaacs, R. (Eds.), 1. Marine Sediments - Gas Content - Congresses. Plenum Press, New York, pp. 99–139.
Coleman, D.D., Risatti, J.B., Schoell, M., 1981. Fractionation of carbon and hydrogen isotopes by methane-oxidizing bacteria. Geochim. Cosmochim. Acta 45, 1033–1037.
Demirbas, A., 2006. The importance of natural gas as a world fuel. Energy Sources, Part B, Econ. Plan. Policy 1, 413–420.
Etiope, G., Schoell, M., 2014. Abiotic gas: atypical, but not rare. Elements 10, 291–296.
Etiope, G., Sherwood Lollar, B., 2013. Abiotic methane on Earth. Rev. Geophys. 51, 276–299.
Feisthauer, S., Vogt, C., Modrzynski, J., Szlenkier, M., Krüger, M., Siegert, M., Richnow, H.-H., 2011. Different types of methane monooxygenases produce similar carbon and hydrogen isotope fractionation patterns during methane oxidation. Geochim. Cosmochim. Acta 75, 1173–1184.
Giunta, T., Labidi, J., Kohl, I., Ruffine, L., Donval, J.-P., Géli, L., Çağatay, M., Lu, H., Young, E., 2021. Evidence for methane isotopic bond re-ordering in gas reservoirs sourcing cold seeps from the Sea of Marmara. Earth Planet. Sci. Lett. 553, 116619.
Giunta, T., Young, E.D., Warr, O., Kohl, I., Ash, J.L., Martini, A., Mundle, S.O., Rumble, D., Pérez-Rodríguez, I., Wasley, M., 2019. Methane sources and sinks in continental sedimentary systems: new insights from paired clumped isotopologues 13CH3D and 12CH2D2. Geochim. Cosmochim. Acta 245, 327–351.
Guggenheim, C., Freimann, R., Mayr, M.J., Beck, K., Wehrli, B., Bürgmann, H., 2020. Environmental and microbial interactions shape methane-oxidizing bacterial communities in a stratified lake. Front. Microbiol. 11, 2374.
Haghnegahdar, M.A., Schauble, E.A., Young, E.D., 2017. A model for 12CH2D2 and 13CH3D as complementary tracers for the budget of atmospheric CH4. Glob. Biogeochem. Cycles 31, 1387–1407.
Hanson, R.S., Hanson, T.E., 1996. Methanotrophic bacteria. Microbiol. Rev. 60, 439–471.
Hayes, J.M., 2001. Fractionation of carbon and hydrogen isotopes in biosynthetic processes. Rev. Mineral. Geochem. 43, 225–277.
Henckel, T., Jäckel, U., Schnell, S., Conrad, R., 2000. Molecular analyses of novel methanotrophic communities in forest soil that oxidize atmospheric methane. Appl. Environ. Microbiol. 66, 1801–1808.
Karl, D.M., Beversdorf, L., Björkman, K.M., Church, M.J., Martinez, A., Delong, E.F., 2008. Aerobic production of methane in the sea. Nat. Geosci. 1, 473–478.
Kinnaman, F.S., Valentine, D.L., Tyler, S.C., 2007. Carbon and hydrogen isotope fractionation associated with the aerobic microbial oxidation of methane, ethane, propane and butane. Geochim. Cosmochim. Acta 71, 271–283.
Labidi, J., Young, E.D., Giunta, T., Kohl, I.E., Seewald, J., Tang, H., Lilley, M.D., Früh-Green, G.L., 2020. Methane thermometry in deep-sea hydrothermal systems: evidence for re-ordering of doubly-substituted isotopologues during fluid cooling. Geochim. Cosmochim. Acta 288, 248–261.
Lenhart, K., Bunge, M., Ratering, S., Neu, T.R., Schüttmann, I., Greule, M., Kammann, C., Schnell, S., Müller, C., Zorn, H., 2012. Evidence for methane production by saprotrophic fungi. Nat. Commun. 3, 1–8.
Liu, Q., Liu, Y., 2016. Clumped-isotope signatures at equilibrium of CH4, NH3, H2O, H2S and SO2. Geochim. Cosmochim. Acta 175, 252–270.
Ma, Q., Wu, S., Tang, Y., 2008. Formation and abundance of doubly-substituted methane isotopologues (13CH3D) in natural gas systems. Geochim. Cosmochim. Acta 72, 5446–5456.
Murrell, J., 2010. The aerobic methane oxidizing bacteria (methanotrophs). In: Handbook of Hydrocarbon and Lipid Microbiology, pp. 1953–1966.
Nothaft, D.B., Templeton, A.S., Rhim, J.H., Wang, D.T., Labidi, J., Miller, H.M., Boyd, E.S., Matter, J.M., Ono, S., Young, E.D., 2021. Geochemical, biological, and clumped isotopologue evidence for substantial microbial methane production under carbon limitation in serpentinites of the Samail Ophiolite, Oman. J. Geophys. Res., Biogeosci. 126, e2020JG006025.
Ono, S., Rhim, J.H., Gruen, D.S., Taubner, H., Kölling, M., Wegener, G., 2021. Clumped isotopologue fractionation by microbial cultures performing the anaerobic oxidation of methane. Geochim. Cosmochim. Acta 293, 70–85.
Ono, S., Wang, D.T., Gruen, D.S., Sherwood Lollar, B., Zahniser, M.S., McManus, B.J., Nelson, D.D., 2014. Measurement of a doubly substituted methane isotopologue, 13CH3D, by tunable infrared laser direct absorption spectroscopy. Anal. Chem. 86, 6487–6494.
Rayleigh, L., 1896. L. Theoretical considerations respecting the separation of gases by diffusion and similar processes. London Edinburgh Dublin Philos. Mag. J. Sci. 42, 493–498.
Reeburgh, W.S., 2007. Oceanic methane biogeochemistry. Chem. Rev. 107, 486–513.
Saunois, M., Bousquet, P., Poulter, B., Peregon, A., Ciais, P., Canadell, J.G., Dlugokencky, E.J., Etiope, G., Bastviken, D., Houweling, S., 2016. The global methane budget 2000–2012. Earth Syst. Sci. Data 8, 697–751.
Schoell, M., 1980. The hydrogen and carbon isotopic composition of methane from natural gases of various origins. Geochim. Cosmochim. Acta 44, 649–661.
Schoell, M., 1988. Multiple origins of methane in the earth. Chem. Geol. 71, 1–10.
Steinle, L., Graves, C.A., Treude, T., Ferré, B., Biastoch, A., Bussmann, I., Berndt, C., Krastel, S., James, R.H., Behrens, E., Böning, C.W., Greinert, J., Sapart, C.J., Scheinert, M., Sommer, S., Lehmann, M.F., Niemann, H., 2015. Water column methanotrophy controlled by a rapid oceanographic switch. Nat. Geosci. 8, 378.
Stolper, D.A., Sessions, A.L., Ferreira, A.A., Neto, E.V.S., Schimmelmann, A., Shusta, S.S., Valentine, D.L., Eiler, J.M., 2014. Combined 13C–D and D–D clumping in methane: methods and preliminary results. Geochim. Cosmochim. Acta 126, 169–191.
Taenzer, L., Labidi, J., Masterson, A.L., Feng, X., Rumble III, D., Young, E.D., Leavitt, W.D., 2020. Low Δ12CH2D2 values in microbialgenic methane result from combinatorial isotope effects. Geochim. Cosmochim. Acta 285, 225–236.
Templeton, A.S., Chu, K.-H., Alvarez-Cohen, L., Conrad, M.E., 2006. Variable carbon isotope fractionation expressed by aerobic CH4-oxidizing bacteria. Geochim. Cosmochim. Acta 70, 1739–1752.
Valentine, D.L., Blanton, D.C., Reeburgh, W.S., Kastner, M., 2001. Water column methane oxidation adjacent to an area of active gas hydrate dissociation, Eel River Basin. Geochim. Cosmochim. Acta 65, 2633–2640.
Wang, D.T., Sattler, A., Paccagnini, M., Chen, F.G., 2020. Method for calibrating methane clumped isotope measurements via catalytic equilibration of methane isotopologues on γ-alumina. Rapid Commun. Mass Spectrom. 34, e8555.
Wang, D.T., Welander, P.V., Ono, S., 2016. Fractionation of the methane isotopologues 13CH4, 12CH3D, and 13CH3D during aerobic oxidation of methane by Methylococcus capsulatus (Bath). Geochim. Cosmochim. Acta 192, 186–202.
Webb, M.A., Miller III, T.F., 2014. Position-specific and clumped stable isotope studies: comparison of the Urey and path-integral approaches for carbon dioxide, nitrous oxide, methane, and propane. J. Phys. Chem. A 118, 467–474.
Whiticar, M.J., 1999. Carbon and hydrogen isotope systematics of bacterial formation and oxidation of methane. Chem. Geol. 161, 291–314.
Whiticar, M.J., 2020. The biogeochemical methane cycle. In: Hydrocarbons, Oils and Lipids: Diversity, Origin, Chemistry and Fate, pp. 669–746.
Whittenbury, R., Phillips, K., Wilkinson, J., 1970. Enrichment, isolation and some properties of methane-utilizing bacteria. Microbiology 61, 205–218.
Widdel, F., Pfennig, N., 1981. Studies on dissimilatory sulfate-reducing bacteria that decompose fatty acids. Arch. Microbiol. 129, 395–400.
York, D., Evensen, N.M., Martınez, M.L., De Basabe Delgado, J., 2004. Unified equations for the slope, intercept, and standard errors of the best straight line. Am. J. Phys. 72, 367–375.
Young, E., Kohl, I., Lollar, B.S., Etiope, G., Rumble, D., Li, S., Haghnegahdar, M., Schauble, E., McCain, K., Foustoukos, D., 2017. The relative abundances of resolved l2CH2D2 and 13CH3D and mechanisms controlling isotopic bond ordering in abiotic and biotic methane gases. Geochim. Cosmochim. Acta 203, 235–264.
Young, Edward D., 2019. A two-dimensional perspective on CH4 isotope clumping: distinguishing process from source. In: Orcutt, Beth N., et al. (Eds.), Deep Carbon: Past to Present. Cambridge University Press, Cambridge, pp. 388–414.
Young, E.D., Rumble, D., Freedman, P., Mills, M., 2016. A large-radius high-mass-resolution multiple-collector isotope ratio mass spectrometer for analysis of rare isotopologues of O2, N2, CH4 and other gases. Int. J. Mass Spectrom. 401, 1–10.
Yung, Y.L., Chen, P., Nealson, K., Atreya, S., Beckett, P., Blank, J.G., Ehlmann, B., Eiler, J., Etiope, G., Ferry, J.G., 2018. Methane on Mars and habitability: challenges and responses. Astrobiology 18, 1221–1242.